Carbohydrate Polymers 207 (2019) 609–618

Contents lists available at ScienceDirect

Carbohydrate Polymers

journal homepage: www.elsevier.com/locate/carbpol

Synthesis of photocurable cellulose acetate butyrate resin for continuous liquid interface production of three-dimensional objects with excellent mechanical and chemical-resistant properties

Rui Hu[a], Bingxue Huang[a], Zhouhang Xue[a], Qingye Li[a], Tian Xia[a], Wei Zhang[a,b,*], Canhui Lu[a,b,*], Huagang Xu[c]

[a] State Key Laboratory of Polymer Materials Engineering, Polymer Research Institute at Sichuan University, Chengdu 610065, China
[b] Advanced Polymer Materials Research Center of Sichuan University, Shishi 362700, China
[c] Quanzhou Yunshang 3D Science & Technology Co. Ltd., Shishi 362700, China

ARTICLE INFO

Keywords:
3D printing
Continuous liquid interface production
Mechanical properties
Photocurable cellulose acetate butyrate
Solvent resistance

ABSTRACT

Three-dimensional (3D) printing parts with excellent resolution and high performance are of great significance for scientific and engineering applications. In this study, a novel photocurable cellulose acetate butyrate (PC-CAB) resin was synthesized for continuous liquid interface production (CLIP) to construct 3D objects with high resolution, tailored mechanical properties, excellent chemical resistance and thermal stability. Particularly, the tensile and flexural strength of the CLIP 3D printed specimen could reach 44.67 and 64.53 MPa, respectively. Their solvent resistance against various organic solvents and strong acidic/basic solutions was evaluated. As expected, the 3D prints could well maintain their structural integrity and exhibited very low swelling ratios owing to the photo-induced chemical crosslinking structure. Notably, even after immersion in methylene chloride or 1.0 M acid/alkali for 3 h, the 3D prints still showed excellent mechanical and thermal properties. Further study demonstrated that when PC-CAB in the CLIP ink was optimized to 20 wt% while the photoinitiator (PI) was 0.5 wt%, complex-structured 3D printed objects with high surface quality could be obtained under specific printing parameters.

1. Introduction

Three-dimensional (3D) printing is a term to describe the technology used for rapid production of 3D objects directly from digital computer aided design (CAD) files (Chua, Leong, & Chu, 2010). This technology, also known as additive manufacturing, has become popular in a wide variety of applications, including tissue engineering (Derby, 2012), materials for energy (Sun et al., 2013), chemistry reactionware (Symes et al., 2012), molecular visualization (Chakraborty & Zuckermann, 2013), microfluidics (Erkal et al., 2014), low-density and high-strength materials (Duoss et al., 2014; Zheng et al., 2014). Nowadays, several 3D printing technologies including fused deposition modeling (FDM), direct ink writing (DIW), selective laser sintering (SLS), stereolithography apparatus (SLA), digital light processing (DLP) and continuous liquid interface production (CLIP) have been developed to meet different requirements.

Among those various 3D printing techniques, photocuring-based 3D printing, including SLA, DLP and CLIP, represent the most precise technologies applied to produce models with an ideal resolution and arbitrarily complex geometry (Zheng et al., 2014). Unlike SLA and DLP, by which a macroscopic object of several centimeters in height may take hours to construct, CLIP enables a model drawn out of the ink in minutes. For example, the gyroid and argyle structures were CLIP printed at 50 cm h^{-1}, reaching a height of ~5 cm in less than 10 min (Tumbleston et al., 2015). And it was possible to tailor the properties of printed objects by simply changing the reactive formulations. Briefly, CLIP printing was realized by repeating the process of projecting an image onto the photocurable inks followed by raising the platform (Tumbleston et al., 2015).

Various photocurable resins including epoxy, polyurethane, polyester and acrylic resin have been employed in SLA and DLP 3D printing (Alhnan et al., 2016; Compton & Lewis, 2014; Duoss et al., 2014; Gurr et al., 2008; Wendel et al., 2010; Williams, James, Chae, & Hunter-Smith, 2015). However, due to the poor performance, most of these printed objects cannot be directly used as parts of devices for some special applications, such as robotics, automotive, aerospace, etc.,

* Corresponding authors at: State Key Laboratory of Polymer Materials Engineering, Polymer Research Institute at Sichuan University, Chengdu 610065, China.
E-mail addresses: weizhang@scu.edu.cn (W. Zhang), canhuilu@263.net (C. Lu).

https://doi.org/10.1016/j.carbpol.2018.12.026
Received 31 May 2018; Received in revised form 9 November 2018; Accepted 10 December 2018
Available online 12 December 2018
0144-8617/

where solvent resistance and mechanical properties are very crucial (Crivello & Reichmanis, 2014). For example, the tensile strength of the 3D prints from bisphenol A-type epoxy acrylate ink was only 5.8 MPa (Cui et al., 2017). Kucherov et al. printed 3D objects via FDM from polylactic acid (PLA), acrylonitrile butadiene styrene (ABS), glycol modified poly(ethylene terephthalate) (PETG). However, they all lost structural integrity in methylene chloride (DCM) medium in just 5 min (Kucherov, Gordeev, Kashin, & Ananikov, 2017). Therefore, it is highly desired to develop new materials compatible with advanced 3D printing technologies that can produce objects with excellent mechanical and chemical resistance properties for various applications.

Cellulose (Fig. S1) is one of the most abundant and inexhaustible natural polymers on earth with many fascinating properties such as biodegradability, reproducibility, biocompatibility, low density, high strength, and ease for chemical modification (Dieter, Brigitte, Hans-Peter, & Andreas, 2005). Cellulose acetate butyrate (CAB) (Fig. S1) is a typical cellulose derivative, whose hydroxyl groups are esterified by acetyl and butyryl groups. It has many unique properties, including excellent solubility, good resistance to moisture and cold, structural and ultraviolet stability (Ceccorulli, Pizzoli, & Scandola, 1993; Wertz, Bédué, & Mercier, 2010). Therefore, CAB has been widely reported as microcapsule materials (Fundueanua et al., 2005; Wang et al., 2011), biodegradable materials (Edgar et al., 2001), compatibilizers (Wibowo, Desai, Mohanty, Drzal, & Misra, 2005), coatings (Miyazaki, Yakou, Nagai, & Takayama, 2003), films and medical materials (Shanbhag, Barclay, Koziara, & Shivanand, 2007; Xu, Huang, Huang, & Yu, 2013). However, CAB has rarely been applied in 3D printing. In this study, we attempted to chemically modify CAB with 2-hydroxyethyl methacrylate (2-HEMA) units to produce a photocurable CAB (PC-CAB) resin with the ambition for its CLIP 3D printing. The results turned out to be quite exciting. Various 3D objects with complex structures could be successfully printed. Impressively, the printing parts demonstrated outstanding mechanical properties and solvent resistance to a series of liquids, such as organic solvents, acid and alkali solutions. It should be noted that the oligomer PC-CAB was soluble in the reactive diluents including 1,6-hexanediol diacrylate (HDDA), trimethylolpropane triacrylate (TMPTA), 1-vinyl-2-pyrrolidone (NVP). Hence, this CLIP compatible photocurable ink could be made in a solvent-free manner.

2. Experimental

2.1. Materials

2-HEMA (96%), isophorone diisocyanate (99%, IPDI), analytical grade hydroquinone (HQ), ditin butyl dilaurate (95%, DBTDL), CAB (hydroxyl group 1–1.6%), HDDA (80%), TMPTA (85%), NVP (99%), were all purchased from Aladdin Co. (Shanghai, China). Bis-(2,4,6-trimethylbenzoyl) phenylphosphineoxide (Irgacure 819), oil red O and carbon black were provided by Sigma-Aldrich Chemical Co. (St. Louis, MO, USA). Analytical grade ethyl acetate, petroleum ether (90–120 °C), DCM, hexane, tetrahydrofuran (THF), ethanol, dimethyl formamide (DMF), *N*-methyl-2-pyrrolidone (NMP), chloroform, toluene, hydrochloric acid, sodium hydroxide were supplied by Chengdu Kelong Co., Ltd. (Sichuan, China). The chemical structures of some chemical reagents were depicted in Fig. S1.

2.2. Synthesis of PC-CAB oligomer

The synthetic route of PC-CAB was shown in Fig. 1. Firstly, 6.28 g IPDI and 4.00 g 2-HEMA were added into a three-necked round-bottomed flask containing 15 g ethyl acetate. Then, 0.20 g DBTDL and 0.20 g HQ were added as the initiator and inhibitor, respectively. And the mixture was magnetically stirred under air atmosphere. After that, the temperature was raised to 75 °C to initiate the reaction. The reaction lasted for 5.5 h at 75 °C under constant magnetic stirring. Next, 26 g CAB well dissolved in 104 g ethyl acetate was added. The reaction lasted for 12 h at 75 °C under constant magnetic stirring to complete the grafting of methacrylate groups. The reaction was terminated by cooling to the room temperature. The primary product was subjected to twice precipitation by petroleum ether. After that, the precipitate was placed in a freeze-drying chamber (FD-1A-50, Biocool, China). The freeze-drying process was maintained at −68 °C for 24 h. Finally, 25.80 g white powder was fabricated by a high speed pulverizer (JP-150 A, Harui, China). And the yield was 80%.

2.3. Preparation of PC-CAB ink and 3D printing

The PC-CAB ink was prepared by homogeneously mixing PC-CAB with reactive diluents (2-HEMA, HDDA and TMPTA) and the photo-initiator Irgacure 819. The ink formulation was showed in Fig. S1.

The CAD designs were drawn using Autodesk 123D Design and exported as STL files. A CLIP 3D printer (500 nm laser, Chengdu Laichuang 3D Science & Technology Co. Ltd.) was employed to produce 3D prints from the PC-CAB ink in a defined area ($60 \times 70 \times 190\ mm^3$). And the smallest feature sizes in the horizontal and vertical planes determined by the optical resolution of the projector and the stepping motor were about 90 and 10 μm, respectively. For 3D printing, the slice thickness was set to 10 μm and the exposure time for each layer was 0.1 s with a light power density of $10\ mW\ cm^2$. The 3D printing was conducted by repeating the process of projecting an image onto the ink followed by raising the platform. Above the dead zone, the curing layer was continuously drawn out of the tank, thereby creating suction forces that constantly renewed the reactive ink. After 3D printing, all products were soaked in an ethanol bath for 5 min to remove the unreacted monomers and then allowed to dry under ambient conditions. Final UV post-treatment (UV-PT) was performed by exposing the 3D prints to UV irradiation (λ 365 nm) for 10 min. Fig. 2a displayed the schematic structure of a CLIP printer and the printing and UV-PT processes for a dog-bone sample, and Fig. 2b showed its possible photo-initiated crosslinking mechanism.

2.4. Characterization

The nuclear magnetic resonance (NMR) spectra of A or B, CAB and PC-CAB were recorded by a 600 MHz ^1H NMR, ^{13}C NMR spectrometer (Bruker BioSpin GabH, Switzerland), in $CDCl_3$ at 296 °C respectively. The Fourier transform infrared spectroscopy (FTIR) spectra of A or B, CAB and PC-CAB were recorded on a Fourier transform infrared spectrometer (Nicolet Magna-IR 550, USA). Gel permeation chromatography (GPC) was performed on a Waters GPC 2410 (Malvern, USA) with a series of Waters Styragel columns in conjunction with a Waters refractive index detector. The mobile phase was THF at a flow rate of $1.0\ mL\ min^{-1}$. The UV–vis spectrum of the Irgacure 819 was measured using a UV-1800 spectrophotometer (Mapada Instruments Co., China). Rheological measurements were performed using a rheometer (AR2000ex, TA Instruments Ltd., Crawley, UK). Thermogravimetric analysis (TGA) was performed with a TG209 F1 instrument (NETZSCH Co., Germany). Dynamic mechanical analysis (DMA) was carried out using a TA Q800 dynamic mechanical analyzer (TA Instruments, USA). Tensile and flexural testing were measured by an Instron 5567 universal testing machine (Instron Co., USA) at a crosshead speed of $20\ mm\ min^{-1}$. The flexural stress-strain properties were measured at a crosshead speed of $2\ mm\ min^{-1}$. Scanning electron microscopy (SEM) was performed on a microscope (JEOL JSM-7500F, Japan) at 10 kV. Laser scanning confocal microscopy (LSCM) was conducted with Zeiss LSM 710 (Carl Zeiss, AG, Germany). The laser source of ~500 nm was blue-green light. Swelling test was performed by immersing the 3D prints in different solvents at room temperature for 24 h. The mass swelling ratio was calculated by the following formula:

$$\text{Mass swelling ratio} = 100 \times (M_t - M_0)/M_0 \quad (1)$$

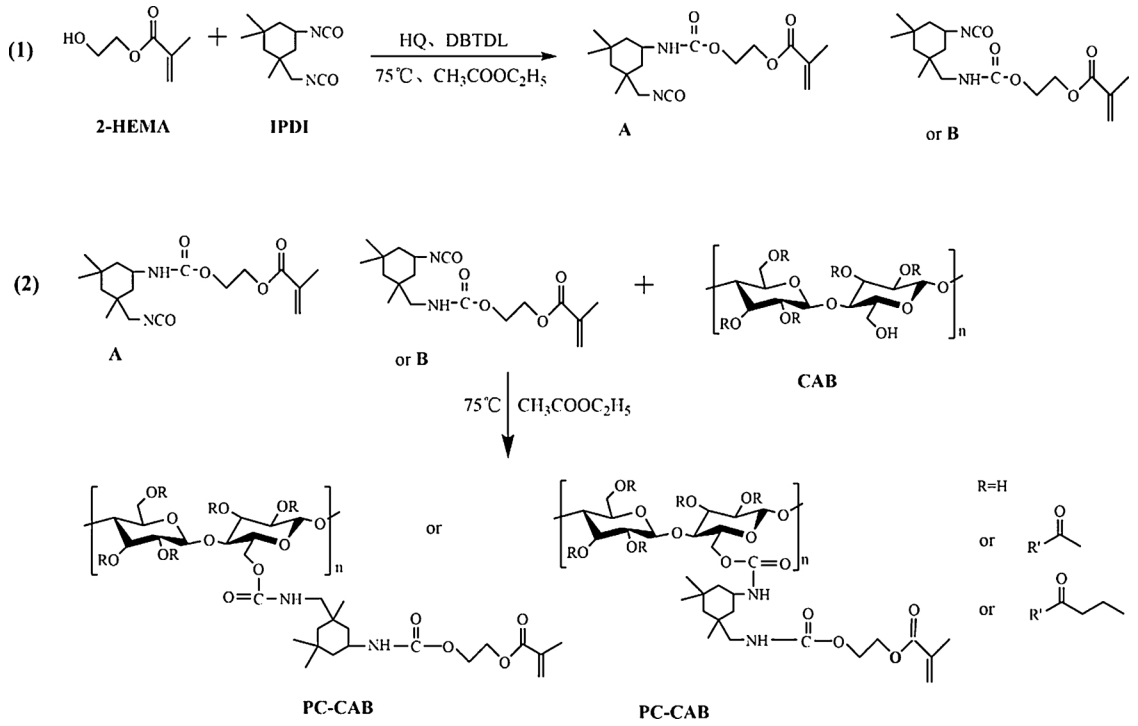

Fig. 1. Scheme for the synthesis of PC-CAB.

Where M_t is the mass of the 3D print after swelling and M_0 is the mass of the dry 3D print before swelling.

3. Results and discussion

3.1. Synthesis of the PC-CAB oligomer

3.1.1. NMR and GPC analysis

The ^{1}H NMR spectra of A or B, CAB, PC-CAB were shown in Fig. 3. The peak at 7.3 ppm was assigned to $CDCl_3$. For A or B, the two peaks at 1.1 and 1.8 ppm (H_7, H_8) were from $-CH_2$ and $-CH_3$ of IPDI molecules (Mishra, Mishra, & Raju, 2009). Additionally, the peak at 7.1 ppm corresponding to −OCONH− was detected (H_5), indicating −NCO of IPDI had reacted with −OH of 2-HEMA (Pardini & Amalvy, 2008). For CAB, the hydrogen protons of cellulose backbone and cellulose ester could be observed at the peaks of 3.5–5.0 and 0.8–2.5 ppm, respectively (Hu et al., 2015). And these peaks were also visible in PC-CAB. For PC-CAB, the $-CH_3$ protons from the methacrylic units (H_1) was at 1.9 ppm. There was an overlapped peak at 4.3 ppm associated with the $-CH_2-$ groups bonded to oxygen in the ester groups, which was designated as H_3 and H_4. The two peaks at 5.6 and 6.1 ppm designated as H_2 (also in A or B) were assigned to the $-OCH_2CH_2OCO-$ groups (Bai, Zhang, Dai,

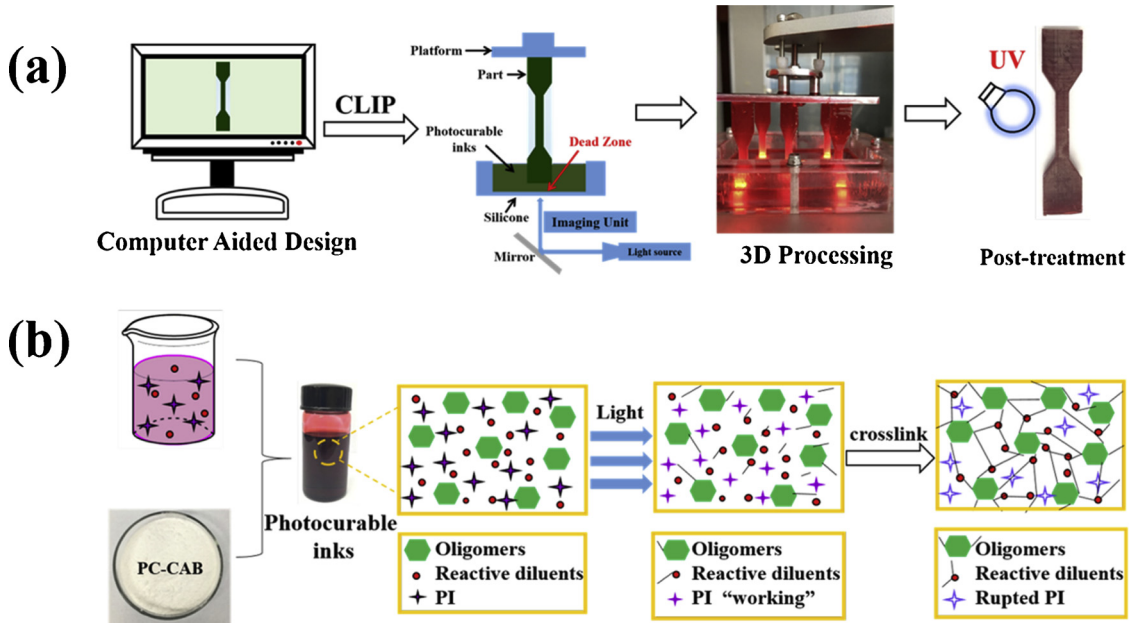

Fig. 2. (a) Scheme of a CLIP printer showing its structures and working mechanism and the printing and UV-PT processes for a dog-bone sample. (b) Reaction mechanism of the PC-CAB ink under light radiation.

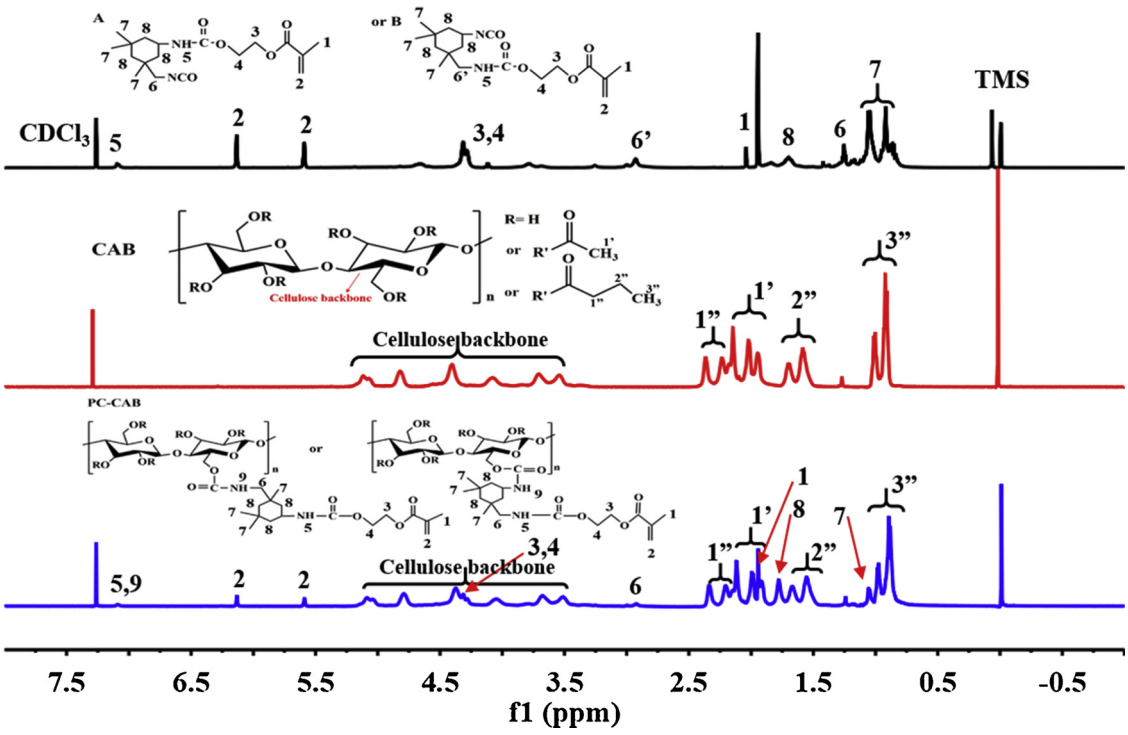

Fig. 3. ^{1}H NMR spectra of A or B, CAB and PC-CAB.

& Li, 2006; Dzunuzovic, Tasic, Bozic, Babic, & Dunjic, 2005; Džunuzović, Tasić, Božić, Jeremić, & Dunjić, 2006). Moreover, a peak at 7.1 ppm was detectable suggesting the successful grafting of A or B onto the CAB backbone (Mishra et al., 2009).

The ^{13}C NMR spectra of A or B, CAB, PC-CAB were shown in Fig. S4. For A or B, the peaks at 136.3, 125.4 and 18.6 ppm were assigned to $-C(CH_3)=CH_2$ (C_5, C_7, C_6) from the 2-HEMA units (Ferrari, Yu, Morbidelli, Hutchinson, & Moscatelli, 2011). The other peaks at 28.0 and 45.2 ppm were attributed to the carbons on the cyclohexyl rings from IPDI units (Mendoza-Novelo, Mata-Mata, Vega-Gonzalez, Cauich-Rodriguez, & Marcos-Fernandez, 2014). These peaks also presented in PC-CAB. And the peaks at 155.2 and 158.8 ppm were attributed to the carbons of −NH−COO− (C_7, C_8) in the PC-CAB chains (Torini, Argillier, & Zydowicz, 2005). These results consistently indicated that PC-CAB had been successfully synthesized via the reaction of −NCO with −OH.

Furthermore, the molecular weight (M_n) of CAB measured by GPC was determined to be 22843, while the M_n of PC-CAB was 27,945 (Table S1), which manifested that something (IPDI, 2-HEMA) had already been grafted onto the CAB backbone. The PC-CAB oligomer only had one main peak at 23 min in its GPC curve (see Fig. S2, other peaks during 30–40 min were ascribed to tetrahydrofuran), suggesting its high purity. In addition, the isocyanate contents of IPDI, A or B and PC-CAB were determined by titrations (the detailed experimental can be found in the supplementary file) to be 24.0%, 10.8%, 0.1%, respectively, in agreement with the reaction mechanism proposed in Fig. 1.

3.1.2. FTIR and solubility analysis

The FTIR spectra of A or B, CAB and PC-CAB were shown in Fig. 4. For the intermediate A or B, the peaks at 2267 and 3354 cm^{-1} were attributed to the −NCO and −N−H stretching, respectively (Wang, Feve, Lam, & Pascault, 1994; Wang, Hu, & Tu, 2008). In the spectrum of CAB, the sharp absorption peak at 1754 cm^{-1} was attributed to the stretching vibration of −COO groups and the intense absorption peak at 3491 cm^{-1} was due to the presence of −OH groups. Whereas PC-CAB exhibited a less intensive −OH peak in this region. And the appearance of the 3383 cm^{-1} peak manifested that −NCO had reacted with −OH to form −NHCOO (Pardini & Amalvy, 2008). The new peaks at 1640 and 802 cm^{-1} were assigned to C=C stretching vibration and =C−H bending vibration respectively, indicating that the acrylate double bonds had been grafted to the CAB backbone.

Excellent solubility was of great importance for PC-CAB to become a photocurable 3D printing material. As shown in Table S2, PC-CAB could be easily dissolved in various reactive diluents including NVP, 2-HEMA, HDDA and TMPTA to form a 3D printing ink, as well as many organic solvents such as DCM, acetone, THF, DMF, etc. Obviously, the introduction of IPDI and 2-HEMA groups as the side chains of PC-CAB had disturbed the ordering of molecules, leading to its excellent solubility.

3.2. Properties of the PC-CAB ink

3.2.1. Rheological properties

The rheological behaviors of the PC-CAB ink were illustrated in Fig. 5. As is well recognized, the viscosity of the printing ink is highly relevant to the printing speed as well as the resolution and appearance of CLIP products (Tumbleston et al., 2015). The PC-CAB ink exhibited a viscosity (η) of ~7144 mPa s that was independent of shear rate over the range of 0.1–10 s^{-1} (Fig. 5a). Due to the strong shear-thinning behaviors, the ink exhibited an apparent viscosity of ~5000 mPa s at the shear rate of ~580 s^{-1}. The shear-induced reorganization of PC-CAB chains to a more stretched conformation would lead to decreased entanglement and thereby viscosity (Malda et al., 2013). The resultant ink displayed good fluidity at ambient conditions, which was crucial for CLIP 3D printing.

Oscillatory measurements at low strains were carried out to assess the viscoelastic properties of the PC-CAB ink. As shown in Fig. 5b, the ink exhibited a plateau value of loss modulus G″ ~44.3 Pa that exceeded the storage modulus G′ ~1.7 Pa by about an order of magnitude at 10–100 Pa shear stress, suggesting its predominantly viscous behavior. Too viscous ink (> 20 wt%) may result in failure of 3D printing as the building plate cannot generate enough suction forces (Gibson, Rosen, & Stucker, 2010). Hence, the 20 wt% PC-CAB ink was chosen for the printing of 3D architectures.

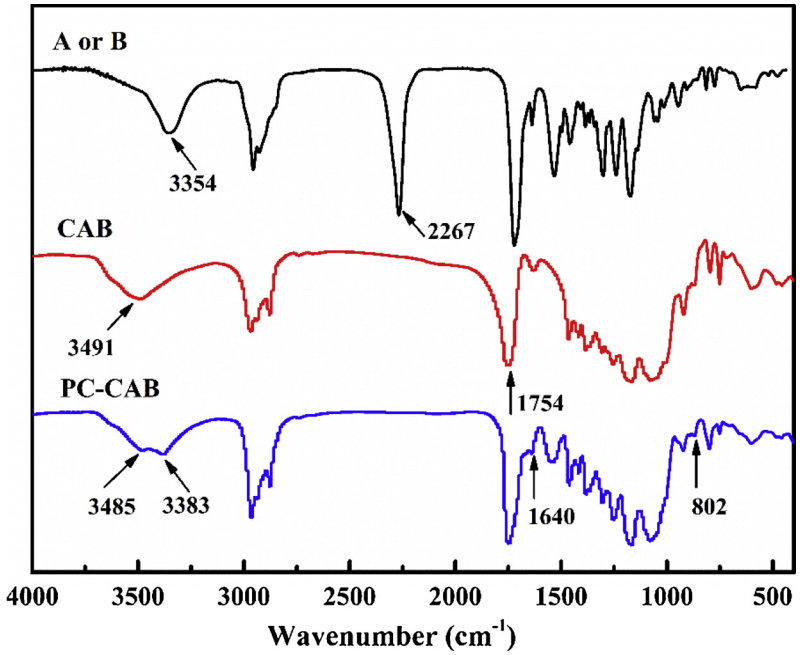

Fig. 4. FTIR spectra of A or B, CAB and PC-CAB.

3.2.2. Mechanical properties of the 3D prints

The mechanical properties of 3D printed parts were compared in Fig. 6 and Table S3. After 10 min UV-PT, the elastic tensile modulus (E) and tensile strength (σ_b) of the 3D prints were increased to 971.93 ± 47.19 MPa and 44.67 ± 1.88 MPa respectively, corresponding to an improvement of nearly 115.54% in modulus and 227.97% in strength as compared with those without post-treatment (WPT). Interestingly, the elongation at break also slightly increased from 5.56% to 8.51% (Table S3), indicating less brittle failure with UV-PT. For the flexural tests, the elastic modulus and flexural strength of the UV-PT samples were 178.82% and 165.27% higher than those of the WPT samples, respectively. These results suggested that UV-PT could further strengthen the interfacial adhesion between the curing layers and increase the crosslinking degree inside each layer. It was important to note that the mechanical properties of the 3D objects were comparable or even higher than those made by extrusion, FDM and DLP, including CAB (extrusion) (E = 1.20–1.26 GPa, σ_b = 25.9–29.3 MPa) (Gindl & Keckes, 2004; Siqueira, Mathew, & Oksman, 2011), ABS (FDM) (E = 1.6 GPa, σ_b = 22–34 MPa) (Rocha et al., 2014), PLA (FDM) (E = 1246–1538 MPa, σ_b = 31–38 MPa) (Afrose, Masood, Iovenitti, Nikzad, & Sbarski, 2016), polyether urethane acrylate (PUA) ink (DLP) (E = 44–56 MPa, σ_b = 4.7–6.6 MPa), polyimide ink (DLP) (E = 1400–3100 MPa, σ_b = 5–25 MPa) (Guo, Ji, Zhang, Wang, & Zhou, 2017), etc.

The influence of UV-PT on the microscopic morphology of the fractured surface of CLIP printed object was examined by SEM (Fig. S4). After UV-PT, the width of the printed stripe decreased from 10.44 to 10.06 mm, while its height changed from 3.98 to 3.95 mm, leading to slight volumetric contraction. Examination on the cross-section of the WPT sample showed a uniform morphology with a few isolated microscale voids (Fig. S4a, b). This could be possibly ascribed to the nonconsistent motions between PC-CAB molecules and cured macromolecules, which resulted in void formation. However, after UV-PT, those voids disappeared (Fig. S4d–f). This was well in line with the tensile testing results that UV-PT could significantly improve the mechanical properties of CLIP printed samples.

3.2.3. Thermomechanical properties and TG/DTG analysis

Thermomechanical properties of the 3D printed parts were characterized by DMA. The loss factor (tanδ) and storage modulus (E') were demonstrated in Fig. 7a. The E' of the 3D prints reached up to 3.21 GPa at room temperature (25 °C) and decreased to 99.72 MPa when the temperature increased to the glass transition temperature (T_g) (125.14 °C). It also suggested that the 3D prints could be employed for long term service at 100 °C (E' = 0.81 GPa) (Guo et al., 2017). The thermal stability of the PC-CAB resin and the resultant 3D prints was

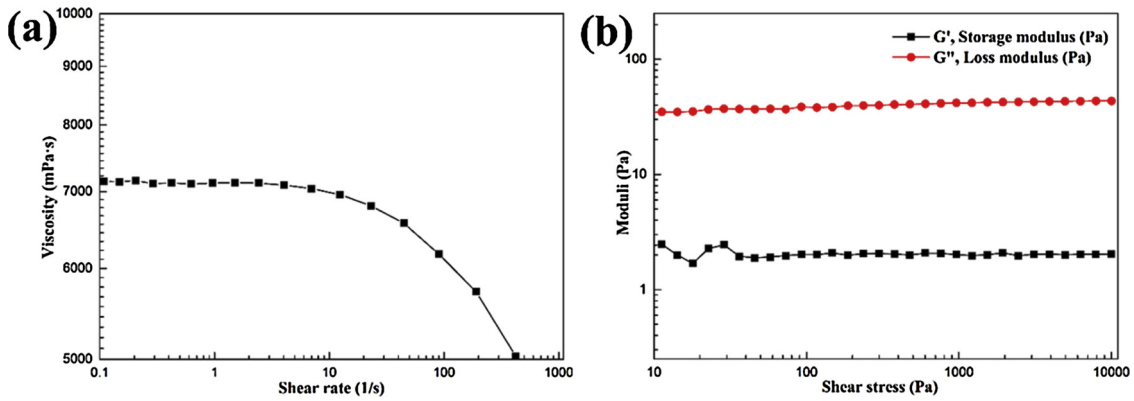

Fig. 5. Log-log plots of (a) apparent viscosity as a function of shear rate, (b) shear storage and loss moduli as a function of shear stress for PC-CAB ink.

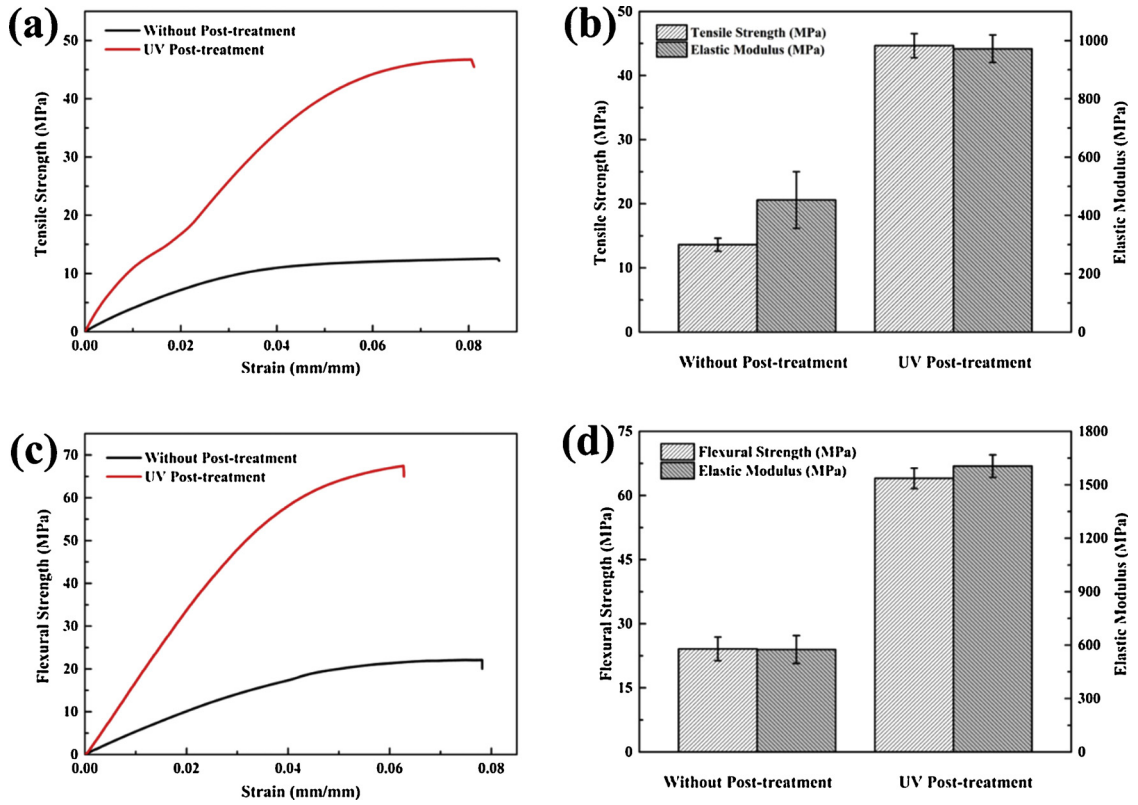

Fig. 6. (a, b) Tensile and (c, d) flexural properties of the samples with and without 10 min UV-PT.

examined by TGA. Both TGA and DTG curves were provided in Fig. 7b, c and Table S4. The initial slight mass loss (about 2–6%) was due to the evaporation of water existed in the samples. A sharp weight loss representing the main pyrolysis step of PC-CAB appeared in the zone (230–400 °C), corresponded to a dominant peak on the DTG curves. At this stage, the molecular chains of CAB fractured and were gradually

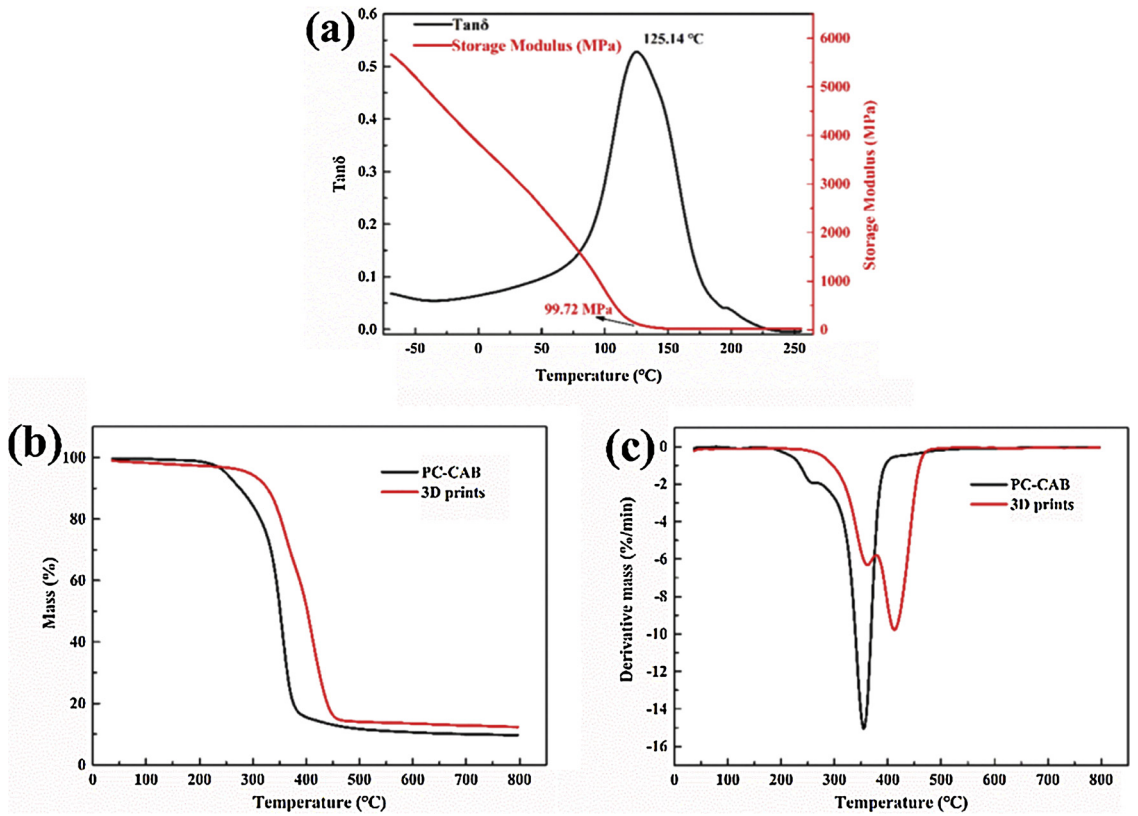

Fig. 7. (a) Thermomechanical properties the 3D prints from DMA analysis (b) TG and (c) DTG curves for PC-CAB and the 3D prints.

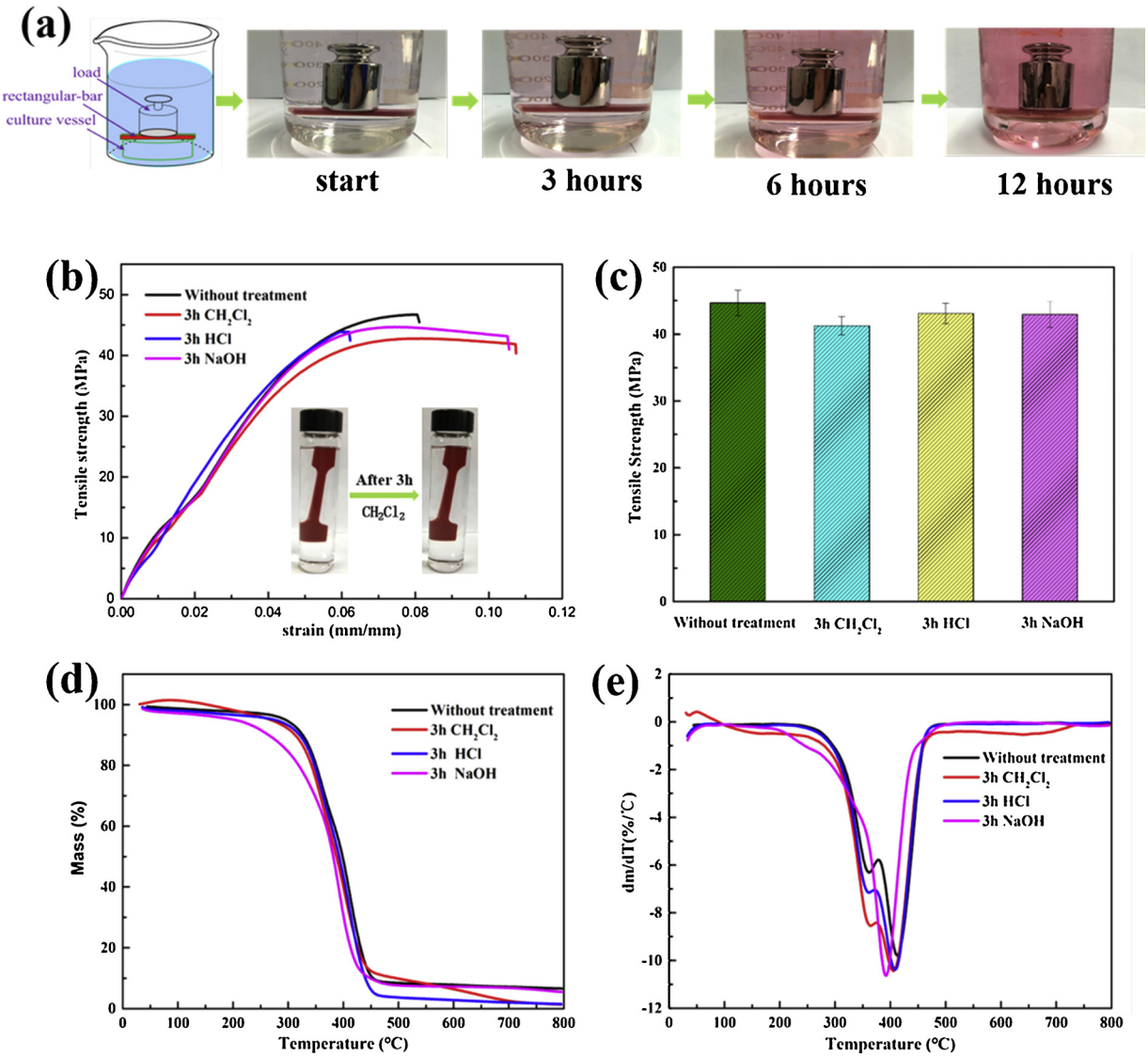

Fig. 8. (a) Evaluation of the overall stability of a 3D printed bar (6 cm × 1 cm × 4 mm) with an appropriate indicator (200 g load) in DCM. Comparative mechanical (b, c) and thermal properties (d, e) of the 3D prints subjected to treatments in DCM, 1.0 M HCl, 1.0 M NaOH solutions for 3 h, respectively. The inset picture in (b) shows the appearance of a dog-bone sample during 3 h immersion in DCM.

transformed to CO_2 and some volatile hydrocarbon species. PC-CAB started to degrade at 228.2 °C with its maximum decomposition rate temperature (T_{max}) of 354.8 °C, whereas the thermo-degradation of 3D prints initiated at 316.1 °C and its T_{max} occurred at 412.2 °C. This could be ascribed to the chemical crosslinking structure that further improved its thermal stability. The sharp weight loss of the 3D prints in the zone (260–480 °C) could be attributed to the volatilization of the Irgacure 819 (Fig. S5a) and some residual active monomers trapped in the cross-linked network during the irradiation process (Jansen & Machado, 2005). The zone (640–700 °C) for the 3D prints was seen as a tail in the DTG curve where the weight loss slowed down. This zone was identified as the thermal decomposition of the char (Chen, Liu, Yu, & Mao, 2011; Chen, Yu, Zhang, & Lu, 2011).

3.2.4. Solvent resistance study on the 3D prints

Solvent resistant assessment and related morphological changes of the 3D prints were demonstrated in Fig. 8 and 9. DCM, a typical polar organic solvent, was selected as a model solvent in the test. As shown in Fig. 8a, a rectangular CLIP printed bar was placed in a beaker filled with DCM and an appropriate indicator (200 g load) was placed on the top of a culture vessel. The indicator could clearly show the point of loss of structural integrity (load drops upon destruction of the bar). The rectangular bar retained its initial shape and was not crushed after a prolonged 3 h experiment. After 6 h, the bar only swelled slightly. Even after 12 h, it was still not crushed yet. However, the DCM became red as the bar had been swelled for a little bit and released some red dyes in the solvent.

To determine the solvent resistance in a quantitative manner, the 3D prints were immersed in DCM, 1.0 M HCl and 1.0 M NaOH solutions for 3 h, respectively. The mechanical and thermal properties of the treated samples were shown in Fig. 8b–e and Table S5. As expected, the tensile and thermal properties of the untreated 3D prints were slightly higher than those of DMC or strong acid/alkali treated ones. After 3 h DCM immersion, SEM studies on the 3D prints' surface and fractured section were performed (Fig. 9). Compared with the untreated ones, the DCM treated sample displayed a porous structure on the surface due to solvent erosion (Fig. 9c, d). However, the fractured surface seemed unchanged (Fig. 9e–g). This revealed that the solvent was not capable to penetrate deeply into the inner part of the 3D prints even after 3 h immersion. Only the surface could be affected by the solvents. Such outstanding solvent erosion resistance was mainly attributed to the covalent cross-linking structure in the 3D prints (Grubbs, Dean, And, &

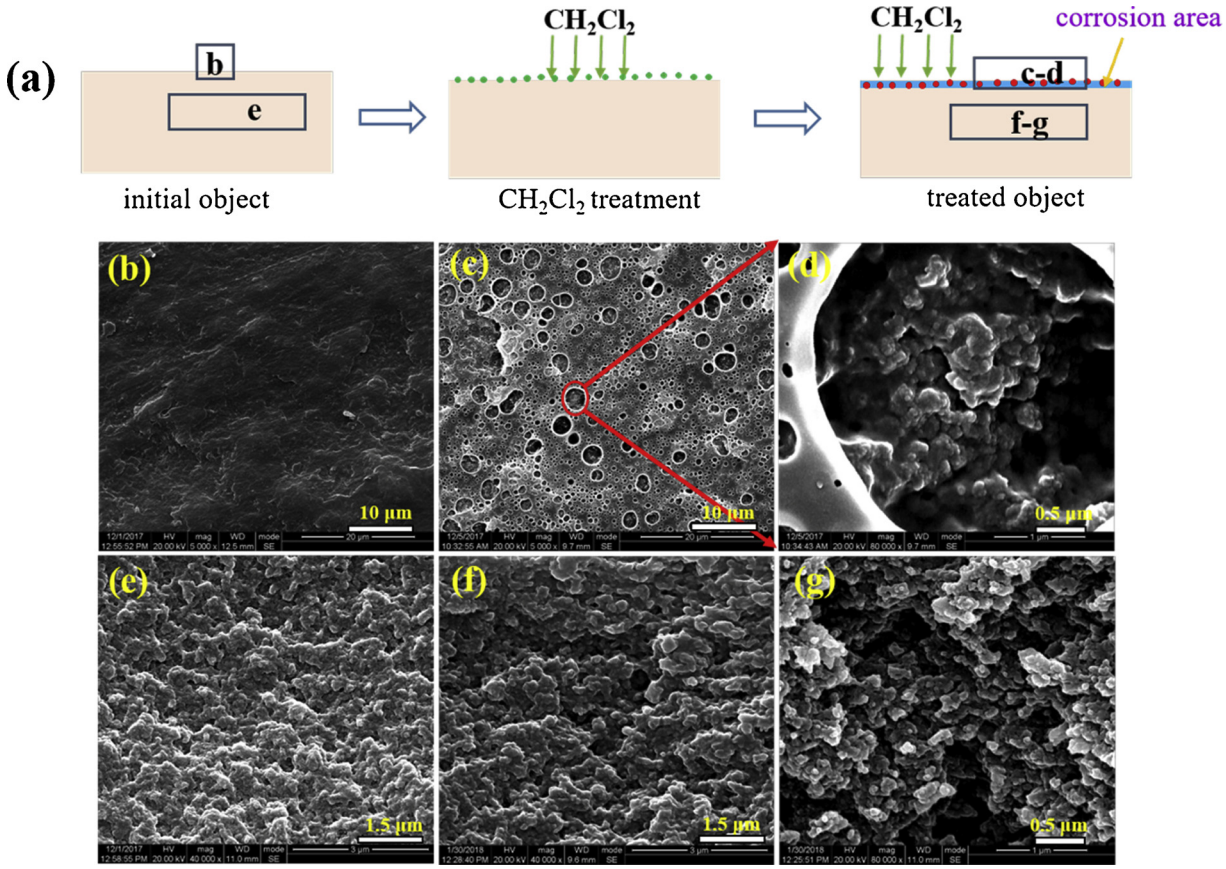

Fig. 9. Investigation on the morphology of solvent-treated samples. (a) Scheme of the locations selected for SEM imaging on the DCM treated sample. (b–g) SEM images of untreated and solvent-treated sample (b, surface of untreated model; c, d, surface of DCM treated model; e, fractured surface of untreated model; f, g, fractured surface of DCM treated model).

Bates, 2000; Montarnal, Capelot, Tournilhac, & Leibler, 2011). Obviously, the CLIP printed PC-CAB was superior in chemical resistance as compared to many other 3D printing materials such as poly(ethylene-2,5-furandicarboxylate) (PEF), PLA, ABS and PETG, which were sensitive to DCM. For example, the FDM printed PEF tablet displayed serious erosion in its inner region when contacting with DCM in just 5 min (Kucherov et al., 2017).

In addition, the swelling ratios of 3D prints soaked in different solvents were also evaluated at room temperature for 24 h (Fig. S6). The 3D prints were immersed in various non-polar or weakly polar organic solvents, polar protic/aprotic organic solvents, strong acid and base. They only showed slight swelling rather than dissolution in organic solvents such as hexane, DMF, toluene, etc. For example, the swelling ratio was only 3.6% when the sample was put in NMP.

3.3. 3D printing resolution and complex architecture from the PC-CAB ink

For CLIP 3D printing of the PC-CAB ink, Irgacure 819 was chosen as the photoinitiator owing to its high reactivity, low cytotoxicity, low cost and strong absorption in the blue-green light region (Fig. S5b) (Maza, 2007). The samples shown in Fig. 10 were all directly printed with UV-PT. The size of the image projected on the tank bottom could be adjusted by setting the parameters of the projector to match the actual model. The printed objects presented remarkable printing resolution with a smooth surface (Fig. 10a). The LSCM image clearly showed that the relative surface roughness of the 3D prints was 2.37 μm (Fig. 10b). As the resolution of 3D printed products directly determined their quality (Stansbury & Idacavage, 2016), the limitation of this PC-CAB ink towards the smallest possible feature size was investigated by printing a 5 mm high column array with varied diameters from 0.5 to 2 mm. As shown in Fig. 10d, all the columns with designed diameters of 2, 1, 0.8 and 0.5 mm were successfully printed, whereas none could be obtained if the diameter was set less than 0.5 mm. Hence, the guaranteed smallest feature size was 0.5 mm. We further applied the PC-CAB ink for the 3D printing of different architectures, such as stars, honeycomb, etc. (Fig. 10c, f–g). Based on different ink formulations, the printed objects may display multiple colors and possess different properties. It was discovered that dark color dyes could improve the printing accuracy to a certain extent by preventing the leakage of light from the desired illuminated area and allowed to control the thickness of each layer during the printing process (Lee et al., 2015).

4. Conclusions

In this study, a novel PC-CAB ink suitable for CLIP 3D printing was developed by using CAB as the raw material which was grafted with 2-HEMA groups in the chain, together with 2-HEMA, HDDA, and TMPTA as reactive diluents, and Irgacure 819 as the photoinitiator. Various complex architectures with high resolution, excellent mechanical properties and solvent resistance were 3D printed in a direct prototype manner. After UV-PT, the tensile and flexural strength of the 3D prints could reach 44.67 and 64.53 MPa, respectively. Furthermore, due to the crosslinking structure generated during CLIP printing, the 3D prints exhibited excellent resistance against a variety of organic solvents. Specifically, the model sample could maintain its shape even after immersing in the aggressive solvent of DCM for 12 h. This simple and high-efficiency CLIP 3D printing of PC-CAB combined with its outstanding mechanical and solvent resistance properties promised it an ideal candidate for various applications such as aviation and automobile manufacturing.

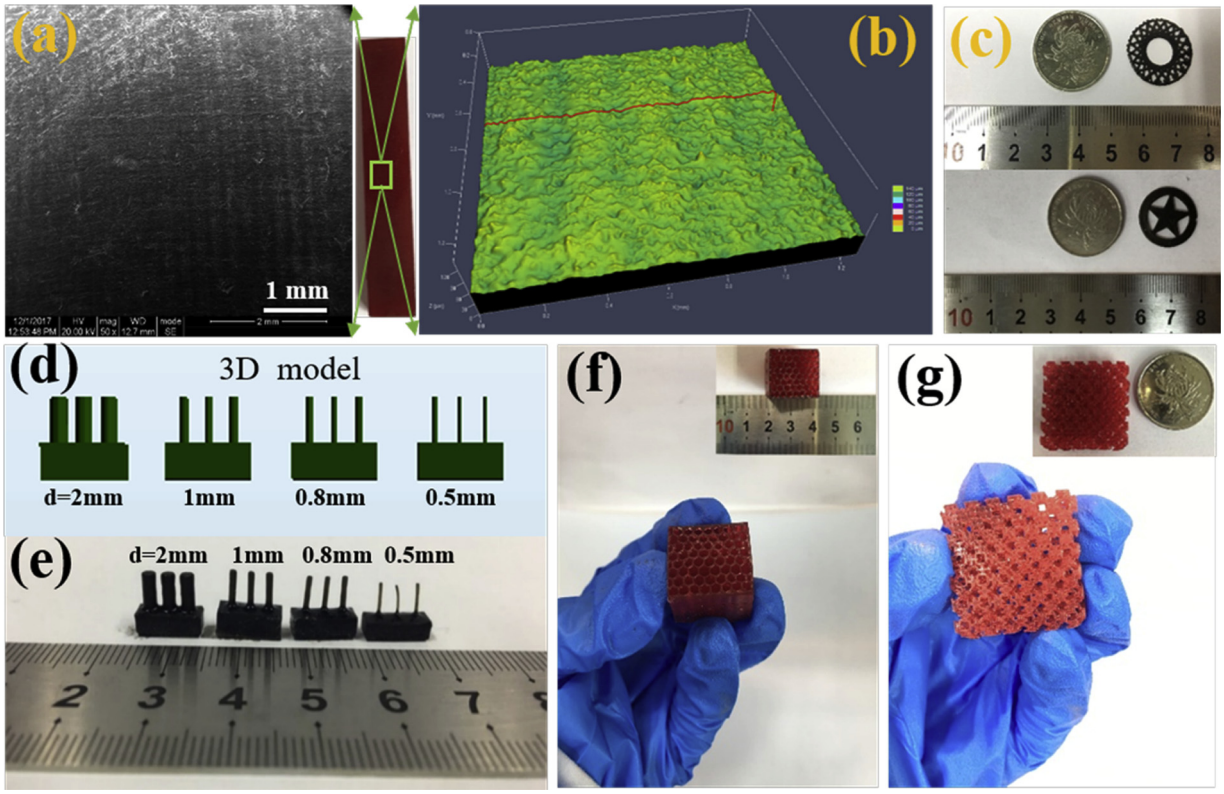

Fig. 10. (a) SEM and (b) LSCM image of the surface finish of a CLIP printed PC-CAB object under different magnifications. (d) 3D models of columns with various diameters and a height of 5 mm for printing accuracy evaluation. (e) The 3D prints from the digital models. (c, f, g) The 3D prints of different architectures. The inset pictures in (f, g) show the macroscopic size of 3D prints.

Acknowledgements

This work was supported by the National Natural Science Foundation of China (51433006, 51473100 and 31500789), Excellent Young Scholar Fund of Sichuan University (20822041B4205), State Key Laboratory of Polymer Materials Engineering (sklpme2016-3-09) and Shishi Municipal Government.

Appendix A. Supplementary data

Supplementary material related to this article can be found, in the online version, at doi:https://doi.org/10.1016/j.carbpol.2018.12.026.

References

Afrose, M. F., Masood, S. H., Iovenitti, P., Nikzad, M., & Sbarski, I. (2016). Effects of part build orientations on fatigue behaviour of FDM-processed PLA material. *Progress in Additive Manufacturing, 1*(1), 21–28.

Alhnan, M. A., Okwuosa, T. C., Sadia, M., Wan, K. W., Ahmed, W., & Arafat, B. (2016). Emergence of 3D printed dosage forms: Opportunities and challenges. *Pharmaceutical Research, 33*(8), 1817–1832.

Bai, C. Y., Zhang, X. Y., Dai, J. B., & Li, W. H. (2006). A new UV curable waterborne polyurethane: Effect of CC content on the film properties. *Progress in Organic Coatings, 55*(3), 291–295.

Ceccorulli, G., Pizzoli, M., & Scandola, M. (1993). Effect of a low-molecular-weight plasticizer on the thermal and viscoelastic properties of miscible blends of bacterial poly(3-hydroxybutyrate) with cellulose acetate butyrate. *Macromolecules, 26*(25), 6722–6726.

Chakraborty, P., & Zuckermann, R. N. (2013). Coarse-grained, foldable, physical model of the polypeptide chain. *Proceedings of the National Academy of Sciences, 110*(33), 13368–13373.

Chen, X., Liu, L., Yu, P. Y., & Mao, S. S. (2011). Increasing solar absorption for photocatalysis with black hydrogenated titanium dioxide nanocrystals. *Science, 331*(6018), 746–750.

Chen, X., Yu, J., Zhang, Z., & Lu, C. (2011). Study on structure and thermal stability properties of cellulose fibers from rice straw. *Carbohydrate Polymers, 85*(1), 245–250.

Chua, C. K., Leong, K. F., & Chu, S. L. (2010). *Rapid prototyping: Principles and applications (with companion CD-ROM)* (3rd edition). World Scientific.

Compton, B. G., & Lewis, J. A. (2014). 3D printing: 3D-printing of lightweight cellular composites. *Advanced Materials, 26*(34), 5930–5935.

Crivello, J. V., & Reichmanis, E. (2014). Photopolymer materials and processes for advanced technologies. *Chemistry of Materials, 26*(1), 533–548.

Cui, K. J., Zhu, C. Z., Zhang, H., Xuan, Q., Zou, W. Z., Zhang, Z. Y., et al. (2017). Blue laser diode-initiated photosensitive resins for 3D printing. *Journal of Materials Chemistry C, 5*(46), 12035–12038.

Derby, B. (2012). Printing and prototyping of tissues and scaffolds. *Science, 338*(6109), 921–926.

Dieter, K., Brigitte, H., Hans-Peter, F., & Andreas, B. (2005). Cellulose: Fascinating biopolymer and sustainable raw material. *Angewandte Chemie International Edition, 44*(22), 3358–3393.

Duoss, E. B., Weisgraber, T. H., Hearon, K., Zhu, C., IV, Metz, W. S., Vericella, T. R., et al. (2014). Three-dimensional printing of elastomeric, cellular architectures with negative stiffness. *Advanced Functional Materials, 24*(31), 4905–4913.

Dzunuzovic, E., Tasic, S., Bozic, B., Babic, D., & Dunjic, B. (2005). UV-curable hyperbranched urethane acrylate oligomers containing soybean fatty acids. *Progress in Organic Coatings, 52*(2), 136–143.

Džunuzović, E., Tasić, S., Božić, B., Jeremić, K., & Dunjić, B. (2006). Photoreactive hyperbranched urethane acrylates modified with a branched saturated fatty acid. *Reactive and Functional Polymers, 66*(10), 1097–1105.

Edgar, K. J., Buchanan, C. M., Debenham, J. S., Rundquist, P. A., Seiler, M. C., Shelton, M. C., et al. (2001). Advances in cellulose ester performance. *Progress in Polymer Science, 26*(9), 1605–1688.

Erkal, J. L., Selimovic, A., Gross, B. C., Lockwood, S. Y., Walton, E. L., Mamara, S. M., et al. (2014). 3D printed microfluidic devices with integrated versatile and reusable electrodes. *Lab on a Chip, 14*(12), 2023–2032.

Ferrari, R., Yu, Y., Morbidelli, M., Hutchinson, R. A., & Moscatelli, D. (2011). ε-Caprolactone-based macromonomers suitable for biodegradable nanoparticles synthesis through Free radical polymerization. *Macromolecules, 44*(23), 9205–9212.

Fundueanua, G., Constantin, M., Esposito, E., Cortesi, R., Nastruzzi, C., & Menegatti, E. (2005). Cellulose acetate butyrate microcapsules containing dextran. *Biomaterials, 26*(20), 4337–4347.

Gibson, I., Rosen, D. W., & Stucker, B. (2010). *Photopolymerization processes. Additive manufacturing technologies: Rapid prototyping to direct digital manufacturing*. Boston, MA: Springer US78–119.

Gindl, W., & Keckes, J. (2004). Tensile properties of cellulose acetate butyrate composites reinforced with bacterial cellulose. *Composites Science and Technology, 64*(15), 2407–2413.

Grubbs, R. B., Dean, J. M., And, M. E. B., & Bates, F. S. (2000). Reactive block copolymers for modification of thermosetting epoxy. *Macromolecules, 33*(26), 9522–9534.

Guo, Y., Ji, Z., Zhang, Y., Wang, X., & Zhou, F. (2017). Solvent-free and photocurable polyimide inks for 3D printing. *Journal of Materials Chemistry A, 5*(31), 16307–16314.

Gurr, M., Hofmann, D., Ehm, M., Yi, T., Kübler, R., & Mülhaupt, R. (2008). Acrylic nanocomposite resins for use in stereolithography and structural light modulation based rapid prototyping and rapid manufacturing technologies. *Advanced Functional Materials, 18*(16), 2390–2397.

Hu, H., Li, H., Zhang, Y., Chen, Y., Huang, Z., Huang, A., et al. (2015). Green mechanical activation-assisted solid phase synthesis of cellulose esters using a co-reactant: Effect of chain length of fatty acids on reaction efficiency and structure properties of products. *RSC Advances, 5*(27), 20656–20662.

Jansen, J. U., & Machado, L. D. B. (2005). A new resin for photocurable electrical insulating varnishes. *Nuclear Instruments and Methods in Physics Research Section B: Beam Interactions with Materials and Atoms, 236*(1), 546–551.

Kucherov, F. A., Gordeev, E. G., Kashin, A. S., & Ananikov, V. P. (2017). Three-dimensional printing with biomass-derived PEF for carbon-neutral manufacturing. *Angewandte Chemie, 129*(50), 16147–16151.

Lee, M. P., Cooper, G. J. T., Hinkley, T., Gibson, G. M., Padgett, M. J., & Cronin, L. (2015). Development of a 3D printer using scanning projection stereolithography. *Scientific Reports, 5*, 9875.

Malda, J., Visser, J., Melchels, F. P., Jüngst, T., Hennink, W. E., Dhert, W. J. A., et al. (2013). 25th Anniversary article: Engineering hydrogels for biofabrication. *Advanced Materials, 25*(36), 5011–5028.

Maza, S. (2007). Evaluation of biocompatible photopolymers I: Photoreactivity and mechanical properties of reactive diluents. *Journal of Macromolecular Science: Part A-Chemistry, 44*(5), 547–557.

Mendoza-Novelo, B., Mata-Mata, J. L., Vega-Gonzalez, A., Cauich-Rodriguez, J. V., & Marcos-Fernandez, A. (2014). Synthesis and characterization of protected oligourethanes as crosslinkers of collagen-based scaffolds. *Journal of Materials Chemistry B, 2*(19), 2874–2882.

Mishra, R. S., Mishra, A. K., & Raju, K. V. S. N. (2009). Synthesis and property study of UV-curable hyperbranched polyurethane acrylate/ZnO hybrid coatings. *European Polymer Journal, 45*(3), 960–966.

Miyazaki, Y., Yakou, S., Nagai, T., & Takayama, K. (2003). Release profiles of theophylline from microspheres consisting of dextran derivatives and cellulose acetate butyrate: Effect of polyion complex formation. *Drug Development and Industrial Pharmacy, 29*(7), 795–804.

Montarnal, D., Capelot, M., Tournilhac, F., & Leibler, L. (2011). Silica-like malleable materials from permanent organic networks. *Science, 334*(6058), 965–968.

Pardini, O. R., & Amalvy, J. I. (2008). FTIR, ^{1}H NMR spectra, and thermal characterization of water-based polyurethane/acrylic hybrids. *Journal of Applied Polymer Science, 107*(2), 1207–1214.

Rocha, C. R., Torrado Perez, A. R., Roberson, D. A., Shemelya, C. M., MacDonald, E., & Wicker, R. B. (2014). Novel ABS-based binary and ternary polymer blends for material extrusion 3D printing. *Journal of Materials Research, 29*(17), 1859–1866.

Shanbhag, A., Barclay, B., Koziara, J., & Shivanand, P. (2007). Application of cellulose acetate butyrate-based membrane for osmotic drug delivery. *Cellulose, 14*(1), 65–71.

Siqueira, G., Mathew, A. P., & Oksman, K. (2011). Processing of cellulose nanowhiskers/cellulose acetate butyrate nanocomposites using sol-gel process to facilitate dispersion. *Composites Science and Technology, 71*(16), 1886–1892.

Stansbury, J. W., & Idacavage, M. J. (2016). 3D printing with polymers: Challenges among expanding options and opportunities. *Dental Materials, 32*(1), 54–64.

Sun, K., Wei, T. S., Ahn, B. Y., Seo, J. Y., Dillon, S. J., & Lewis, J. A. (2013). 3D printing of interdigitated Li-ion microbattery architectures. *Advanced Materials, 25*(33), 4539–4543.

Symes, M. D., Kitson, P. J., Yan, J., Richmond, C. J., Cooper, G. J. T., Bowman, R. W., et al. (2012). Integrated 3D-printed reaction ware for chemical synthesis and analysis. *Nature Chemistry, 4*(5), 349–354.

Torini, L., Argillier, J. F., & Zydowicz, N. (2005). Interfacial polycondensation encapsulation in miniemulsion. *Macromolecules, 38*(8), 3225–3236.

Tumbleston, J. R., Shirvanyants, D., Ermoshkin, N., Janusziewicz, R., Johnson, A. R., Kelly, D., et al. (2015). Continuous liquid interface production of 3D objects. *Science, 347*(6228), 1349–1352.

Wang, B., Tang, Q., Hong, N. N., Song, L., Wang, L., Shi, Y. Q., et al. (2011). Effect of cellulose acetate butyrate microencapsulated ammonium polyphosphate on the flame retardancy, mechanical, electrical, and thermal properties of intumescent flame-retardant ethylene-vinyl acetate copolymer/microencapsulated ammonium polyphosphate/polyamide-6 blends. *Applied materials & Interfaces, 3*(9), 3754–3761.

Wang, F. C., Feve, M., Lam, T. M., & Pascault, J. P. (1994). FTIR analysis of hydrogen bonding in amorphous linear aromatic polyurethanes. I. Influence of temperature. *Polymer Physics, 32*(8), 1305–1313.

Wang, F., Hu, J. Q., & Tu, W. P. (2008). Study on microstructure of UV-curable polyurethane acrylate films. *Progress in Organic Coatings, 62*(3), 245–250.

Wendel, B., Rietzel, D., Kühnlein, F., Feulner, R., HüLder, G., & Schmachtenberg, E. (2010). Additive processing of polymers. *Macromolecular Materials & Engineering, 293*(10), 799–809.

Wertz, J. L., Bédué, O., & Mercier, J. P. (2010). *Cellulose science and technology.* CRC Press.

Wibowo, A. C., Desai, S. M., Mohanty, A. K., Drzal, L. T., & Misra, M. (2005). A solvent free graft copolymerization of maleic anhydride onto cellulose acetate butyrate bioplastic by reactive extrusion. *Macromolecular Materials and Engineering, 291*(1), 90–95.

Williams, C., James, A., Chae, M. P., & Hunter-Smith, D. J. (2015). 3D printing in clinical podiatry: A pilot study and review. *Journal of Foot and Ankle Research, 8*(2), O41.

Xu, W., Huang, W. B., Huang, X. G., & Yu, C. Y. (2013). A simple fiber-optic humidity sensor based on extrinsic Fabry-Perot cavity constructed by cellulose acetate butyrate film. *Optical Fiber Technology, 19*(6), 583–586.

Zheng, X., Lee, H., Weisgraber, T. H., Shusteff, M., Deotte, J., Duoss, E. B., et al. (2014). Ultralight, ultrastiff mechanical metamaterials. *Science, 344*(6190), 1373–1377.